ARTICLE

Atomic Simulation of Structure and Deformation's Influence on the Mechanical Properties of Single-walled Carbon Nanotubes

Xiang-gui Ni*, Yu Wang, Zhong Zhang, Xiu-xi Wang

CAS Key Laboratory of Mechanical Behavior and Design of Materials, University of Science and Technology of China, Hefei 230026, China

(Dated: Received on August 6, 2005; Accepted on November 8, 2005)

Tensile deformation behaviors and the Poisson's ratio of single-walled carbon nanotubes (SWCNTs) are numerically studied, using the molecular dynamics (MD) method. Effects of several structural features of crystal cells of SWCNTs, i.e., the size, chirality and strain, on their mechanical properties are analyzed systematically. The simulations indicate that Armchair SWCNTs (8, 8)-(22, 22) and Zigzag SWCNTs (9,0)-(29,0) can be stretched by 35%-38% and 20%-27% without sign of plasticity, respectively. The Young's modulus of SWCNTs under tension ranges from 960 GPa to 750 GPa as their radii increase. The Young's modulus of zigzag SWCNTs is higher than that of armchair SWCNTs. Additionally, three SWCNTs (9,9), (12,6) and (16,0) are investigated to obtain their Poisson's ratio under tensile and compressive loading. The results show that the Poisson's ratio of nanotubes decreases generally as the strain increases. Under the same tensile strain, the Poisson's ratio decreases as the chiral angles of SWCNTs decrease, while their Poisson's ratios increase under the same compressive strain.

Key words: Single-walled carbon nanotube, Chiral dependence, Size dependence, Strain dependence, Poisson's ratio

I. INTRODUCTION

Carbon nanotubes (CNTs) discovered by Iijima [1] as by-products of fullerene synthesis have attracted growing interest due to their novel structures and exceptional properties, perhaps mainly due to the potentially promising important applications in which nanotubes can be used. Their uses include atomic force microscopy (AFM) tips, field emitters, nanoscale electric devices, hydrogen storage, and so on. Carbon nanotubes will likely be used in the development of ultra-strong CNT-reinforced composites, due to the exceptional mechanical properties of CNTs [2-4]. For example, the axial Young's modulus of CNTs could be as high as 1 TPa (assuming a shell thickness of 0.34 nm for all the Young's moduli mentioned in this work). Their tensile strength may approach 100 GPa, almost twenty times that of high strength steel alloys. Finally, the deformation of a single-walled carbon nanotube (SWCNT) is completely reversibly subjected to a large strain of almost 40% [5,6].

An accurate characterization of the properties of individual CNTs is essential for the investigation of crystalline ropes of CNTs and CNT-reinforced composites. Hence, the mechanical properties of CNTs have been the challenging subject of a number of experimental as well as theoretical studies. It is generally recognized that the mechanical properties of CNTs are dependent upon their structural makeup.

So far, there mainly have been two experimental methods for measuring the mechanical properties of CNTs: transmission electron microscopy (TEM) and atomic force microscopy (AFM). Since Treacy *et al.* first experimentally determined the Young's modulus of multi-walled carbon nanotubes (MWCNTs) [7], other researchers have continued to obtain experimental results, as shown in Table I, and the work is ongoing. All these experimental results have shown that CNTs have exceptional mechanical properties, and could therefore be used in the synthesis of highly resistant composites.

However, it is difficult to characterize the mechanical properties accurately due to the limitations of current experimental techniques in manipulating nanoscale materials. In particular, there have been significant technical difficulties in determining other elastic moduli, such as Poisson's ratio and bulk and shear moduli. Hence, atomic simulation for assessing mechanical properties of CNTs has been regarded as a powerful tool. The *ab initio* calculation [14], the tight-binding (TB) method [15], and the molecular dynamics (MD) method with empirical potentials [5] have been used quite extensively. In general, the *ab initio* calculation gives more accurate results than the MD method, but it is computationally intensive and prohibitive to use in larger models. Recent achievements in atomic simulation on CNTs can be seen in Table II.

Quantum/molecular mechanics and continuum mechanics have been highly developed to describe material properties at the atomic, molecular and macro scales. To better model mechanical properties of CNTs, several new approaches linking the quantum/molecular

*Author to whom correspondence should be addressed. E-mail: xianggui@ustc.edu.cn

TABLE I Experimental results of elastic moduli for carbon nanotubes

Researchers	Experimental method	Object	Young's modulus / TPa	Shear modulus / TPa
Treacy *et al.* [7]	TEM	Thermal vibration of cantilevered tubes	1.8±0.9	
Wong *et al.* [8]	AFM	Bending anchored nanotubes	1.28±0.59	
Krishnan *et al.* [9]	TEM	SWCNTs	0.9-1.6	
Salvetat *et al.* [10]	AFM	Individual SWCNT ropes	0.81±0.41	0.1
Yu *et al.* [11,12]	AFM tips under SEM	A MWCNT	0.27-0.95	
Demczyk *et al.* [13]	TEM	Bending carbon nanotubes	0.91	

TABLE II Recent achievements of atomic simulations on CNTs

Researchers	Numerical method	Object	Young's modulus/TPa	Shear modulus/TPa	Poisson's ratio
Lier *et al.* [16]	*ab initio*	(9, 0)	1.14		0.11
Sanchez-Portal *et al.* [14]	*ab initio*	MWCNTs, SWCNTs	1 for MWCNTs		0.14 for (*n*, *n*) 0.19 for (10, 0) 0.18 for (8, 4)
Hernandez *et al.* [15]	Nonorthogonal TB method	SWCNTs	1.22-1.26		0.26
Yakobson *et al.* [17]	MD method	SWCNTs	1.07 (5.5 for the thickness of 0.066 nm)		
Lu *et al.* [18]	Empirical force-constant model	Nanotubes, nanoropes	0.97	0.45	0.28
Popov *et al.* [19]	Force-constant lattice-dynamics model	SWCNTs	From 0.85 to 0.20 with the increasing diameter		0.17
Mylvaganam *et al.* [6]	MD method [20-22]	Armchair tubes	0.72 (3.96 for the thickness of 0.0617 nm)		0.15
		zigzag tubes	0.89 (4.88 for the thickness of 0.0617 nm)		0.19
Our research group [23,24]	MD method	SWCNTs under compression	From 1.5 to 1.3 with the increasing radius		

mechanics and continuum mechanics have been proposed, detailed in Table III.

From the above studies, it can be seen that, although some results indicate the elastic properties of CNTs are insensitive to their sizes or chiralities [15,18,26,30,31], most reports demonstrate a size and chiral dependence of the Young's modulus and Poisson's ratio.

This work aims to understand the deformation behavior of SWCNTs under tensile loading and to analyze the effects of the size, chirality and deformation on the mechanical properties of SWCNTs, using the MD method with Tersoff-Brenner potentials [21].

II. STRUCTURE OF CARBON NANOTUBES

Experimental studies on the structure of carbon nanotubes by the high resolution electron microscopy have proved that MWCNTs are made of several or tens of SWCNT layers, coaxially by a spacing 0.34 nm. A SWCNT can be formed by creatively folding a graphene sheet to form a hollow tube composed of carbon hexagons. Because the graphene hexagonal lattice can be rolled at different angles, the geometry of a particular nanotube is described in terms of the unit cell of the carbon nanotubes, as shown in Fig.1. The atomic arrangement of carbon nanotubes can be indexed by a pair of integers (n,m), which are called the chiral indices, corresponding to a chiral vector $\mathbf{C}_h=n\mathbf{a}_1+m\mathbf{a}_2$ on the graphite plane, where $\mathbf{a}_1$ and $\mathbf{a}_2$ are unit vectors on the two-dimensional hexagonal lattice. The chiral angle is the angle between $\mathbf{C}_h$ and $\mathbf{a}_1$. The lattice vector $\mathbf{T}$ is the basic translational vector in the axial direction of the tube. The vector $\mathbf{T}$ is normal to the chiral vector $\mathbf{C}_h$, and is determined automatically if $\mathbf{C}_h$ is specified. The integers (n,m) uniquely determine the size of a SWCNT. The fundamental carbon nanotubes are classified into three categories in terms of their chirality: zigzag (m=0), armchair (n=m), and chiral (arbitrary n and m). On giving (n,m), the structural parameters of a SWCNT can be determined. Once the size of the vector $\mathbf{T}$ is given, its initial spatial configuration of the structure can be constructed for the computational simulation. A number of studies have shown that the chirality of SWCNTs greatly effects their physical properties.

TABLE III Recent studies of approaches linking multi-scale theories on CNTs

Researchers	Numerical method	Object	Young's modulus/TPa (with increasing tube diameter)	Poisson's ratio (with increasing tube diameter)
Odegard *et al.* [25]	Equating the molecular potential energy of nano-materials to the mechanical strain energy of a representative continuum model	A graphene sheet	1.54	
Zhang *et al.* [26]	Continuum mechanics approach directly incorporating interatomic potentials	SWCNTs	0.694	
	Visualizing a SWCNT as an effective "stick-spiral" system and using force equilibrium approach in the framework of molecular mechanics	SWCNTs	1.06-0.94	0.26-0.16
Shen *et al.* [28]	Energy approach in the framework of molecular mechanics	SWCNTs	0.93-1.06	0.26-0.16
Natsuki *et al.* [29]	Model of truss structures linked by inter-atomic potentials	SWCNTs MWCNTs	2.2-0.45 1.6-0.8	0.33-0.27

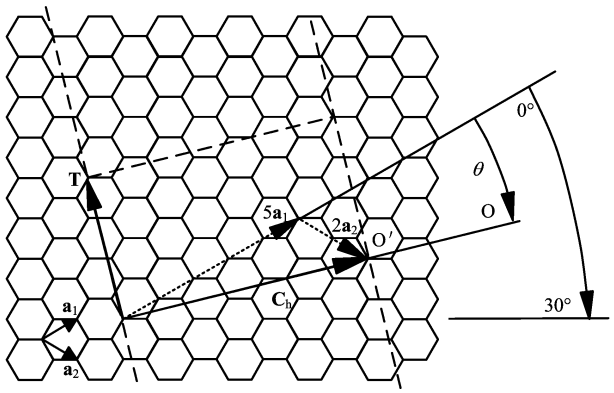

FIG. 1 Unit cell and chiral vector for a (5, 2) SWCNT.

III. MOLECULAR DYNAMICS (MD) METHOD

Newton dynamics functions are employed to determine the variation of instantaneous location and velocity of each atom in the MD method. In our molecular dynamics simulation program, the atomic interaction is represented by the second-generation multi-body Tersoff-Brenner potential [21], which can accurately describe covalent bonds between carbon atoms and efficiently simulate the atomic hybridization and breaking of covalent bonds.

A third-order prediction-correction algorithm is adopted for kinetic equations [32], for it can give more precise results and only the variables used at a moment are saved by computer. Berendsen thermostats are used to control the temperature during the simulation [22]. The environment's temperature is kept at 0.01 K, which avoids the thermal kinetic effect. In the simulation process, the initial configuration of SWCNTs is relaxed to reach the equilibrium state, where the energy of system is minimized. Each loading step includes the following processes: fixing five layers of atoms at one end and shifting five layers of atoms at the other end by 0.001 nm in the axial direction while other atoms are free, then relaxing the carbon nanotube for about 0.3 ps to reach a new equilibrium state and get a new configuration.

IV. ELASTIC AND PLASTIC PROPERTIES OF SWCNTS UNDER TENSION

Eleven zigzag SWCNTs (9,0)-(29,0) and seven armchair SWCNTs (8, 8)-(22, 22) are simulated. The whole simulation process includes 2000 steps. The simulation shows that under small tensile strain, the sections of SWCNTs keep their circular shape, and their micro hexagonal honeycomb arrangements are still regular. As the strain increases, all hexagons are stretched in the axial direction. If the applied external load is unloaded before the strain reaches a critical value (also called fracture strain or breaking strain), the hexagonal arrangements of SWCNTs return to the initial state and no bond breaking or defects occur. After the strain exceeds the fracture strain, some C−C covalent bonds may break so that a few small defects occur in the wall of the nanotube, which leads to an irregular arrangement of atoms. With load being exerted continually, the zone of atomistic disorder is rapidly expanded in axial and circumferential directions of the tube, defects increase quickly, and the tube is weakened. Similar peculiar phenomena of SWCNTs under tension were also observed by Yakobson *et al.* [17] and Mylvaganam *et al.* [6], using the earlier and current Tersoff-Brenner potential respectively.

Figure 2 shows that the fracture strain for armchair and zigzag SWCNTs varies from 35% to 38% and from 20% to 27% with the increasing diameter of nanotubes, respectively. This implies armchair SWCNTs have bet-

ter tensile resistance than zigzag SWCNTs. Yakobson *et al.* [17] investigated nanotubes (7,7), (11,3) and (13,0), using the earlier Tersoff-Brenner potential [33]. They exhibited fracture strains between 30% and 40%. Mylvaganam *et al.* [6] found the fracture strain was 40% for a armchair nanotube (10,10) and 22% for a zigzag nanotube (17,0), using the current Tersoff-Brenner potential [21]. These results are consistent with those shown in Fig.3. However, Belytschko *et al.* [34] reported that the fracture strains varied from 10% to 15% for the zigzag SWCNT (20,0), and the fracture strain of the armchair SWCNT (12,12) was 18.7%, using a molecular mechanics model. Unfortunately, there are still no experimental results for SWCNTs to confirm these numerical results. Up to now, only tensile tests for MWCNTs have been reported by Yu *et al.* [11,12]. They demonstrated fracture strains from 10% to 13% for the majority of MWCNTs, even as low as 2% for some MWCNTs.

We further investigated the elastic modulus of armchair and zigzag SWCNTs under tension. As seen from Fig.3, the range of the Young's modulus is about 750-960 GPa, which agrees well with the experimental result of 1.28±0.59 TPa reported by Treacy *et al* [7]. Furthermore, the Young's modulus decreases as the radii increase, which is consistent with the trend described in Popov's illustration [19], but references [27,35] gave some different results. Clearly there is more work to be done, and further effort should be invested in the research.

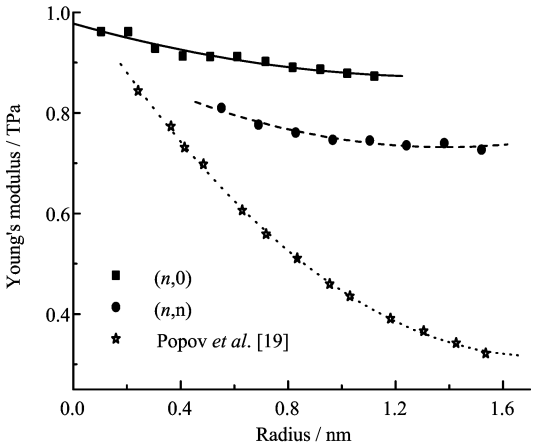

FIG. 3 Relation between Young's modulus and radius of armchair SWCNTs (n, n) and zigzag SWCNTs (n,0).

Figure 3 also indicates that the Young's modulus has a noticeable dependence on the chirality of SWCNTs. The Young's modulus of the zigzag SWCNTs is higher than that of the armchair SWCNTs. This result can be explained by examining the nanostructure features of the crystal cell of zigzag and armchair SWCNTs. From Fig.4, it is clear that among three covalent bonds connecting with an atom, one bond directly parallels the loading direction (axial direction Z) and the other two bonds form an angle with the loading direction in the zigzag SWCNT, while one bond is perpendicular to the loading direction and the other bonds form an angle with the loading direction in the armchair SWCNT. Thus, due to the structure's mechanics, an armchair SWCNT deforms more easily than a zigzag SWCNT when the same external load is exerted. Compared with studies presented by Li *et al.* [35] using the molecular mechanics model, the present results are in agreement with those in respect of the chiral dependence.

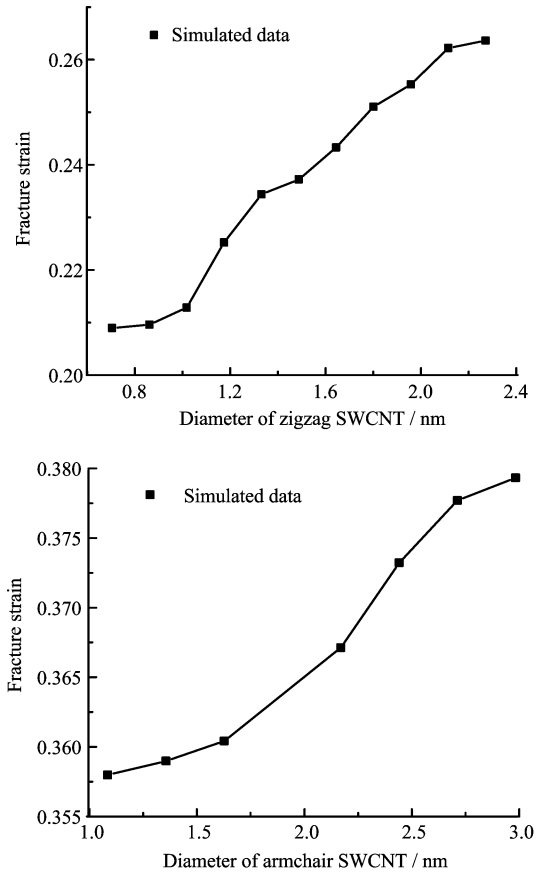

FIG. 2 Fracture strain *vs.* diameter for SWCNTs.

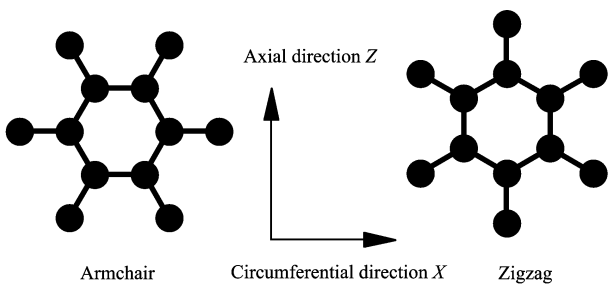

FIG. 4 Crystal cell of armchair and zigzag SWCNTs.

TABLE IV Model parameters for armchair nanotubes

Chiral indices (n, m)	Computational length/nm	Chiral angle/(°)	Diameter/nm
(9,9)	6.404	30	1.2230
(12,6)	6.173	19.1	1.2467
(16,0)	6.890	0	1.2584

V. CALCULATION OF THE POISSON'S RATIO OF SWCNTS

Although many of the simulation studies have calculated the Poisson's ratio of SWCNTs, few systematic calculations have been done for the nanotubes of the same diameter. Furthermore, the dependence of strain and chirality on the Poisson's ratio of SWCNTs up to now has been missed in most studies.

In this section, three nanotubes (9,9), (12,6), (16,0) are investigated. Their model parameters are shown in Table IV. Their diameters and computational lengths are taken as almost the same. Because only their chiral angles are different, the differences in the Poisson's ratio given by the calculations can be regarded as the effects of only the chiral angle on the Poisson's ratio.

The Poisson's ratio is defined as

$$\nu = -\frac{\Delta d/d}{\Delta l/l} \tag{1}$$

Where d is the initial diameter of a carbon nanotube, Δd is the averaged change of diameter of the unstrained part of a carbon nantuobe, l is the initial length of unstrained part of a carbon nanotube, and Δl is the change in length.

Many studies have indicated that SWCNTs buckle when the compressive strain reaches about 6% [24], while they break when the tensile strain reaches about 30% [6,17]. Therefore, we only pay attention to the elastic deformations of less than 3.5% for nanotubes under compression and below 15% for nanotubes under tension. Thus, we chose 300 loading steps for compression and 900 steps for tension in our simulation.

A. Poisson's ratio of SWCNTs under compression

Figure 5 describes the change trend of the Poisson's ratio of selected nanotubes with different chiral angles under compression. The results show that the Poisson's ratio of nanotubes of the larger chiral angles, such as (9,9) and (12,6), decreases with increasing compressive strain. The Poisson's ratio of the zigzag nanotube (16, 0) seems to slightly increase as the compressive strain increases. Furthermore, the Poisson's ratio of nanotubes with the larger chiral angles are lower than those of nanotubes with the smaller chiral angles. For these three nanotubes under compression, their Poisson's ratios change from roughly 0.22 to 0.34. The range of the Poisson's ratio is almost the same as reported by Shintani *et al.* [36].

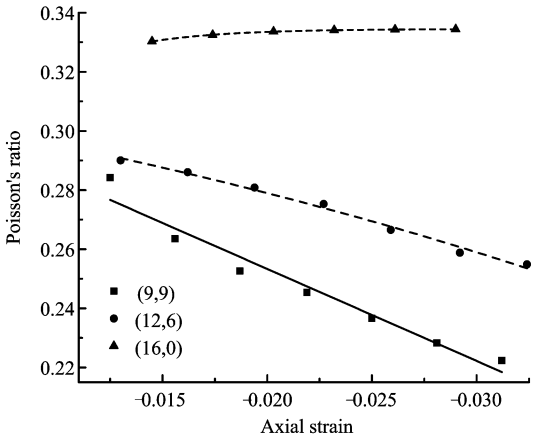

FIG. 5 Poisson's ratio of SWCNTs of different chiral angles under compression.

From Fig.4, we have explained that an armchair SWCNT deforms more easily than a zigzag SWCNT when the same external load is exerted, in Section IV. It can be concluded that the crystal cell of an armchair SWCNT is formed by rotating that of a zigzag SWCNT by 90°. That is to say, for nanotubes with the same diameter under the same axial strain, the circumferential deformation of a zigzag SWCNT is larger than that of an armchair SWCNT. Therefore, the Poisson's ratio of a zigzag SWCNT is larger than that of an armchair SWCNT.

The deformation details of the crystal cell of the armchair SWCNT (9,9) and the zigzag SWCNT (16,0), under the same compressive strain, are depicted in Fig.6. We find that the strain of the 1st side is close to that of the 2nd side. However, the 1st side is an oblique edge relative to the axial direction of the nanotube, therefore it bears a lower axial stress than the 2nd side. Moreover, it makes the 3rd side compress. As a result, the whole circumferential strain of armchair nanotubes is smaller than that of zigzag nanotubes. Thus, the Poisson's ra-

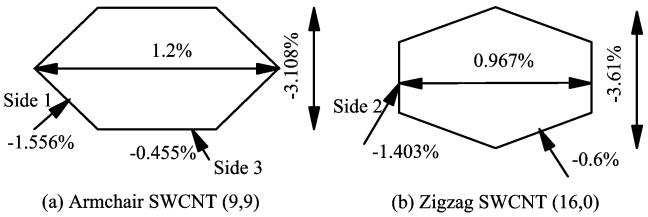

FIG. 6 Compressive deformation details of the crystal cell of SWCNTs in the 200th loading step.

tio of armchair nanotubes is smaller than that of zigzag nanotubes.

B. Poisson's ratio of SWCNTs under tension

Figure 7 shows the Poisson's ratio of selected SWCNTs of different chiral angles under tension. It can be seen that, under the same tensile strain, the Poisson's ratio of nanotubes with larger chiral angles is larger than that of nanotubes with smaller chiral angles. Furthermore, all their Poisson's ratios decrease as the tensile strain increases. When the chiral angles of SWCNTs decrease, their Poisson's ratios decrease under the same tensile strain, while their Poisson's ratios increase under the same compressive strain. Shintani *et al.* [36] also found that with varying chiral angles, the change trend of the Poisson's ratios of SWCNTs are opposite under tension and under compression. We can also observe that the Poisson's ratios of SWCNTs under tension range from 0.28 to 0.05, much lower than the values under compression. Why does this phenomenon occur? In simulation employing the molecular dynamic method, a key factor, which causes the same SWCNT to have different properties under tension and under compression, may be that the Tersoff-Brenner potential function representing the atomic interaction of C−C bonds provides different relationships between the force and the strain under tension or then under compression. As shown in Fig.8, the slope of the force-strain curve under compression is larger than that of under tension. This results in the different deformations of the crystal cells of SWCNTs under compression and under tension.

Figure 9 shows the deformation details of the crystal cells of SWCNTs (9,9) and (16,0) in the 700^{th} loading step. From Fig.9 (a), it can be seen that the axial deformation of the SWCNT (9,9) owes to the elongation of oblique sides and the increasing of angle 1, and there is a larger circumferential deformation. While the axial deformation of the SWCNT (16,0) mainly owes to the straight side, and there is a little circumferential deformation. Therefore, the Poisson's ratio of the armchair SWCNT (9,9) is larger than that of the zigzag SWCNT (16,0) under the same tensile strain.

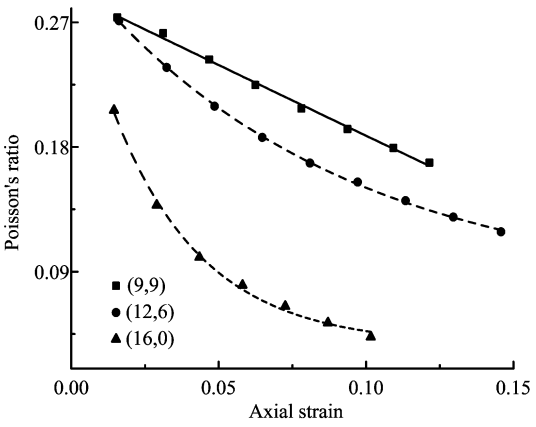

FIG. 7 Poisson's ratio of SWCNTs of different chiral angles under tension.

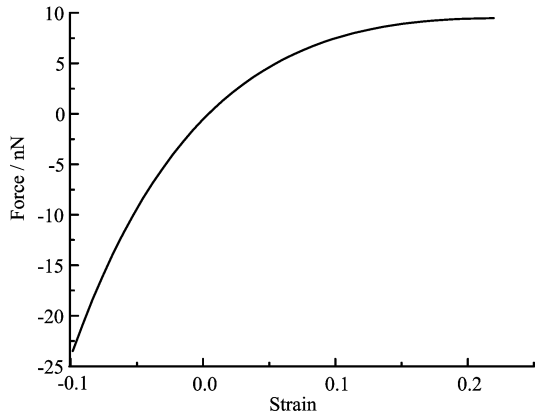

FIG. 8 Relation between the force and the strain provided by the Tersoff-Brenner potential.

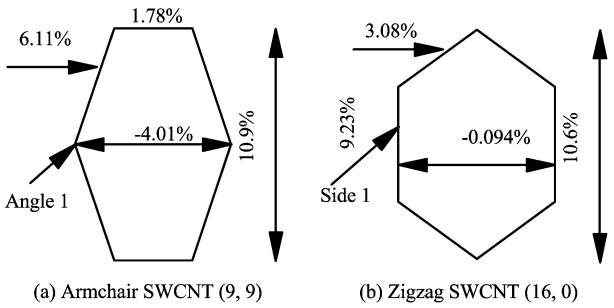

FIG. 9 Tensile deformation details of the crystal cells of SWCNTs in the 700^{th} loading step.

VI. CONCLUSION

This study investigated the elastic and plastic deformation behavior of SWCNTs under tension and the Poisson's ratio of SWCNTs under compression and under tension, respectively, using the MD method with the second-generation multi-body Tersoff-Brenner potential. The simulations show that armchair SWCNTs (8,8)-(22,22) can be stretched by 35%-38% with no sign of plasticity, or atomic rearrangement, while zigzag SWCNTs (9,0)-(29,0) can be only stretched by 20%-27%. The range of the Young's modulus of stretched SWCNTs under tension is about 750-960 GPa, and the Young's modulus of a SWCNT decreases as its radius increases. The Young's modulus of the zigzag SWCNTs is higher than that of the armchair SWCNTs.

Investigating three SWCNTs (9,9), (12,6) and (16,0) under tension and compression, we concluded that the Poisson's ratio of nanotubes decreases as the strain increases. When the chiral angles of SWCNTs decrease,

their Poisson's ratios decrease under the same tensile strain, while their Poisson's ratios increase under the same compressive strain.

These phenomena are explained from the viewpoint of the structural mechanics of the crystal cells of SWCNTs. Our studies show that the deformation and the micro structural characteristic of the configuration of a SWCNT have great influence on its mechanical properties.

VII. ACKNOWLEDGMENT

This work was supported by the National Natural Science Foundation of China (10502047) and Postdoctoral Foundation of China (No.2005038166).

[1] S. Iijima, Nature **354**, 56 (1991).
[2] D. Qian, E. C. Dickey, R. Andrews and T. Rantell, Appl. Phys. Lett. **76**, 2868 (2000).
[3] D. Qian, G. J. Wager, W. K. Liu, M. F. Yu and R. S. Ruoff, Appl. Mech. Rev. **55**, 495, (2002).
[4] M. C. Weisenberger, E. A. Grulke, D. Jacques, *et al*. J. Nanosci. Nanotech. **3**, 535 (2003).
[5] B. I. Yakobson and C. J. Brabec, Bernholc J. Phys. Rev. Lett. **76**, 2511 (1996).
[6] K. Mylvaganam and L. C. Zhang, Carbon **42**, 2025 (2004).
[7] M. M. J. Treacy, T. W. Ebbesen and J. M. Gibson, Nature **381**, 678 (1996).
[8] E. W. Wong, P. E. Sheehan and C. M. Lieber, Science **277**, 1971 (1997).
[9] E. Krishnan, T. W. Dujardin, P. N. Ebbesen, Yianilos and M. M. J. Treacy, Phys. Rev. B **58**(20), 14013 (1998).
[10] J. P. Salvetat, G. A. D. Briggs, J. M. Bonard, *et al*. Phys. Rev. Lett. **82**(5), 944, (1999).
[11] M. F. Yu, O. Lourie, M. J. Dyer, K. Moloni, T. F. Kelly and R. S. Ruoff, Science **287**, 637 (2000).
[12] M. F. Yu, B. S. Files, S. Arepalli and R. S. Ruoff, Phys. Rev. Lett. **84**, 5552 (2000).
[13] B. G. Demczyk, Y. M. Wang, J. Cumings, *et al*. Mater. Sci. Eng. A **334**: 173, (2002).
[14] D. Sanchez-Portal, E. Artacho, J. M. Soler, A. Rubio and P. Ordejon, Phys. Rev. B **59**, 12678 (1999).
[15] E. Hernandez, C. Goze, P. Bernier and A. Rubio, Phys. Rev. Lett. **80**, 4502 (1998).
[16] G. V. Lier, C. V. Alsenoy, V. V. Doren and P. Geerlings, Chem. Phys. Lett. **326**, 181 (2000).
[17] B. I. Yakobson, M. P. Campbell, C. J. Brabec, *et al*. Comp. Mater. Sci. **8**, 341 (1997).
[18] J. P. Lu, Phys. Rev. Lett. **79**, 1297 (1997).
[19] V. N. Popov, V. E. Van Dorena and M. Balkanskib, Solid State Comm. **114**, 395 (2000).
[20] J. Tersoff, Phys. Rev. Lett. **56**, 632 (1986).
[21] D. W. Brenner, O. A. Shenderova, J. Harrison, S. J. Stuart, B. Ni and S. B. Sinnott, J. Phys: Cond. Matter. **14**, 783 (2002).
[22] W. G. Hoover, Phys. Rev. A, 1985, 31: 1695.
[23] X. G. Ni, Y. Wang, X. X. Wang and Q. Cheng, Chin. J. Chem. Phys. **18**, 45 (2005).
[24] Y. Wang, X. X. Wang, X. G. Ni and H. A. Wu, Comp. Mater. Sci. **32**, 141 (2005).
[25] G. M. Odegard, T. S. Gates, L. M. Nicholson, *et al*. Composites Sci. Tech. **62**, 1869 (2002).
[26] P. Zhang, Y. Huang, P. H. Geubelle, P. A. Klein and K. C. Hwang, Int. J. Solids Struct. **39**, 3893 (2002).
[27] T. Chang and H Gao., J. Mech. Phys. Solids **51**, 1059 (2003).
[28] L. X. Shen and J. Li, Phys. Rev. B **69**(4), 045414 (2004).
[29] T. Natsuki, K. Tantrakarn and M. Endo, Appl. Phys. A: Mater. Sci. Proc. **79**(1), 117 (2004).
[30] R. Saito, G. Dresselhaus and M. S. Dresselhaus, *Physical Properties of Carbon Nanotubes*, London: Imperial College Press, (1998).
[31] E. Hernandez, C. Goze, P. Bernier and A. Rubio, Appl. Phys. A. **68**, 287 (1999).
[32] J. M. Haile, *Molecular Dynamics Simulation-Elementary Methods*, New York: Wiley InterScience, 159 (1997).
[33] D. W. Brenner, Phys. Rev. B **42**, 9458 (1990).
[34] T. Belytschko, S. P. Xiao, G. C. Schatz and R. S. Ruoff, Phys. Rev. B **65**, 235430 (2002).
[35] C. Y. Li and T. W. Chou, Int. J. Solids Struct. **40**, 2487 (2003).
[36] K. Shintani and T. Narita, Surf. Sci. **532-535**, 862 (2003).